Omics approach to reveal the effects of obesity on the protein profiles of the exosomes derived from different adipose depots

Minting Chen
Hong Kong Baptist University
Fan Zhang
Guangzhou University of Traditional Chinese Medicine: Guangzhou University of Chinese Medicine
Baisen Chen
Hong Kong Baptist University
Condon Lau
City University of Hong Kong
Chuying Huo
Hong Kong Baptist University
Quanbin Han
Hong Kong Baptist University
Tao Su
Guangzhou University of Traditional Chinese Medicine: Guangzhou University of Chinese Medicine
Hiu Yee Kwan (hykwan@hkbu.edu.hk)
Hong Kong Baptist University https://orcid.org/0000-0002-6088-7323

Research Article

Keywords:

Posted Date: April 19th, 2022

DOI: https://doi.org/10.21203/rs.3.rs-1544257/v1

Abstract

Background: Obesity affects the cargo packaging of the adipocyte-derived exosomes. Furthermore, adipocytes in different adipose tissues have different genetic makeup, the cargo contents of the exosomes derived from different adipose tissues under obesity should be different, and hence their impacts on the pathophysiological conditions.

Methods and Results: iTRAQ-based quantitative proteomics show that obesity has more prominent effects on the protein profiles of the exosomes derived from subcutaneous adipose tissue (SAT-Exos) in the diet-induced obesity (DIO) mice than those derived from epididymal adipose tissue (EAT-Exos) and visceral adipose tissue (VAT-Exos). The differential expressed proteins (DEPs) in SAT-Exos and VAT-Exos are mainly involved in metabolism. Subsequent untargeted metabolomic and lipidomics analysis reveal that injection of these SAT-Exos into the B6/J-Rab27a-Cas9-KO mice significantly affects the mouse metabolism such as fatty acid metabolism. Some of the DEPs in SAT-Exos are correlated with fatty acid metabolism including ADP-ribosylation factor and mitogen-activated protein kinase kinase kinase-3. Pathway analysis also shows that SAT-Exos affect adipocyte lipolysis and glycerophospholipid metabolism, which is in parallel with the enhanced plasma levels of fatty acids, diglycerides, monoglycerides and the changes in glycerophospholipid levels in DIO mice.

Conclusion: Our data provide evidence to suggest SAT-Exos contribute to the changes in plasma lipid profiles under obesity conditions.

Introduction

Exosomes are nanometer-size, membrane-bound extracellular vesicles that mediate cell-to-cell communications locally and systemically by delivering different functional cargos such as proteins, lipids, long noncoding RNAs and microRNAs to the recipient cells and affect the cellular biological process [1–2].

The contents of the exosomes that are derived from pre-adipocytes and mature adipocytes are different. Studies show that exosomes derived from preadipocyte have higher level of signaling fatty acids and adipogenesis markers when compared to those derived from mature adipocytes [3]. Besides, the cargo contents of the exosomes derived from mature adipocytes are also different between non-obese and obese subjects. Under obesity conditions, adipocytes have hypertrophic and hyperplastic growth that led to adipocyte dysfunction that dysregulates the assembly and sorting of the biological contents in the exosomes [4–7]. Hence, these exosomal content may underlie the pathophysiologic changes of the recipient targets under obesity conditions. Many studies have demonstrated that under obesity conditions, the exosomes derived from mature adipocytes have crucial roles in mediating obesity associated comorbidities such as type 2 diabetes, vascular diseases, liver steatosis, inflammation and cancers [8–12]. For example, in the ob/ob mice, the adipocyte derived exosomes induce insulin resistance and increase pro-inflammatory cytokine secretion [13]. Besides, exosomes secreted from the adipocytes

also increase the hypertrophic growth of the adipocytes in an autocrine manner by enhancing lipogenesis [14].

However, adipocytes in different adipose depots have different genetic backgrounds [15–17]. That is, the genes are of fat depot-specific expression patterns [17] and are differentially expressed in different adipocytes such as subcutaneous and visceral adipocytes. A study shows that the adipocytes in the visceral adipose tissues (VAT), subcutaneous adipose tissues (SAT) and epididymal adipose tissues (EAT) only share 1907 genes in common, with the genetic profile in SAT is distinct from those in VAT and EAT [16]. Many of these differentially expressed genes are correlated with various obesity-related traits [17]. Since the genetic makeup of the adipocytes in different adipose tissues are different, the exosomal contents in the exosomes that are derived from these adipose tissues, and hence their biological and pathological impacts should also be different. Nevertheless, less studies have differentiated the biological and pathological effects of these exosomes under obesity conditions.

Exosomes carry a broad array of transmembrane proteins and soluble proteins [1]. The exosomal proteins constitute an essential part of the human adipose tissue secretome [7, 18]. A proteome analysis has identified 897 adipokines in the adipocyte-derived exosomes, which have strong association to human metabolic diseases [18]. Besides, many of these exosomal proteins are implicated in various signaling pathways, integrin signaling and membrane mediated processes [18]. Indeed, the majority of the proteins implicated in metabolism can be found in the adipocyte derived exosomes [19].

In this study, we aimed to compare the impacts of obesity on the protein profiles of the exosomes that are derived from different adipose tissues. Then, we separately injected these exosomes into constitutive Rab27a knockout mice (B6/J-Rab27a-Cas9-KO) and compared the metabolic profiles of these mice with diet-induced obesity mouse models. The data would suggest the differential contributions of these exosomes to the metabolic profiles and the pathophysiology of obesity. Besides, correlations of the differential exosomal proteins to the metabolic changes under obesity conditions would suggest potential novel targets for exosome-based therapy for obesity.

Methods And Materials

Establish diet induced obesity (DIO) mouse models

Male C57BL/6 mice (4-5 weeks old) were purchased from the Laboratory Animal Services Centre, Chinese University of Hong Kong. Mice were housed in ventilated cages in the animal room at the Hong Kong Baptist University, with a 12 h light-dark cycle. The animal studies were approved by the Research Ethics Committee at Hong Kong Baptist University and the Department of Health in the Hong Kong Special Administration Region. All the animal experiments were conducted according to the ethical standards and national guidelines. The mice were randomly selected to have either control diet (D12450J Research Diets), or high fat diet (D12762 Research Diets) for 8 weeks to induce obesity. Both diet and water were supplied *ad libitum*. Body weight of the mouse was recorded every week.

Extraction of adipose tissue derived exosomes from DIO mouse models

After dietary intervention, DIO mice were scarified, and adipose tissues were dissected. Visceral adipose tissue (VAT) was the perirenal fat dissected from the fat pad surrounding the kidneys. Subcutaneous adipose tissue (SAT) were the bilateral superficial subcutaneous white adipose deposits between the skin and muscle fascia just anterior to the lower segment of the hind limbs. Epididymal adipose tissues (EAT) was dissected from the fat pad over the epididymis. These adipose tissues were separately cultured in medium prepared by exosome depleted fetal bovine serum. The adipose tissue derived exosomes were then purified form the conditioned medium with differential ultracentrifugation method [20]. Transmission electron microscopy (TEM), dynamic light scattering (DLS) and expression of exosomal markers CD63 and CD81 were done to confirm the authenticity of the purified exosomes.

Transmission electron microscopy (TEM)

The preparation of exosomes for TEM was done as described [21]. Briefly, exosomes in the conditioned medium were isolated as described above and were mixed with 2.5% glutaraldehyde in 0.1 M sodium cacodylate solution (pH 7.0) for 1 h at 4°C. Sodium cacodylate (0.1 M) was prepared and was adjusted to pH 7.4. The exosomes were rinsed with the sodium cacodylae and was post-fixed with osmium tetroxide for 1 hr at 4°C before incubating with graded acetone on shaker. Then the exosomes were subsequently incubated with solutions of different ratios of acetone and low viscosity embedding mixture. Exosomes were then double stained with uranyl acetate and lead citrate before being observed under TEM (Philips CM100 Transmission Electron Microscope).

Dynamic light scattering (DLS)

The extracted exosomes were diluted to 0.1 μg/μl using Dulbecco's phosphate-buffered saline and then transferred into a cuvette. The measurement was started after the laser and temperature equilibrium of the Photon Correlation Spectroscopy (PHOTOCOR) was stabilized. Temperature control, refractive index, scattering angle and laser wavelength were standardized. Exosomes were identified by their diameters.

Western blot analysis

Proteins were extracted in lysis buffer containing 150 mM sodium chloride, 1% Triton X-100, 0.5% sodium deoxycholate, 0.1% SDS,50 mM Tris (pH 8.0), and protease and phosphatase inhibitors, incubated on ice for 30 min before centrifugation. Quantification of protein was performed using the Pierce™ BCA Protocol Assay kit (Thermo Scientific™ 23227). Equal amount of the protein samples was denatured before separated on 10% sodium dodecyl sulfate–polyacrylamide (SDS-PAGE) gel and transferred onto polyvinylidene difluoride (PVDF) membranes. The transferred proteins were incubated overnight at 4°C with either CD63 or CD81 antibody. Immunodetection was accomplished using horseradish peroxidase-conjugated secondary antibody, followed by enhanced chemiluminescence (ECL) detection system (Amersham).

iTRAQ-based quantitative proteomics

Proteins were extracted from the exosomes, proteolysis and peptide labeling were then performed. The peptide samples were dissolved in 0.5M TEAB and added to the corresponding iTRAQ labeling reagent. Different sample peptides had different iTRAQ labelling. For peptide fractionation, Shimadzu LC-20AB liquid phase system was used. A 5 μm 4.6x250 mm Gemini C18 column for liquid phase separation of the samples was used. The samples were reconstituted with mobile phase A (5% ACN pH 9.8), eluted at 1 mL/min flow rate with mobile phase B (95% ACN, pH 9.8). The peptides separated by liquid phase chromatography were passed to a tandem mass spectrometer Q Exactive HF-X MS (Thermo Fisher Scientific, San Jose, CA) for data dependent acquisition (DDA) mode detection. The protein databases NCBInr compiled by NCBI (National Center for Biotechnology Information) were used for Blast searches. Protein quantification was done with software lQuant integrated with Mascot Percolator to quantitatively analyze the labeled peptides with isobaric tags and provide significance measures. PSMs were pre-filtered at PSM-level FDR of 1%. The pathway enrichment analysis was performed with differentially expressed proteins with p-value less than 0.05.

LC-MS/MS based untargeted metabolomics

Mouse serum metabolites were extracted by methanol and acetonitrile (2:1, v/v), and internal standards were used. The metabolites were resuspended in 50% methanol. After centrifugation, supernatants were subjected to LC-MS analysis with Waters 2D UPLC coupled to Q-Exactive mass spectrometer with a heated electrospray ionization source and controlled by the Xcalibur 2.3 software program (Thermo Fisher Scientific). Chromatographic separation was performed on a Waters ACQUITY UPLC BEH C18 column. In the positive mode, mobile phase A was 0.1% formic acid and mobile phase B was acetonitrile. In negative mode, mobile phase A was 10 mM ammonium formate and mobile phase B was acetonitrile. The data quality was evaluated by the repeatability of QC sample detection. The data were processed by Compound Discoverer 3.1 (ThermoFisher Scientific) and R package metaX software. Compounds with coefficient of variation (CV) of the relative peak area greater than 30% were deleted. For univariate analysis, data were subjected for fold change analysis and T-test and p-value was corrected for false discovery rate (FDR) to obtain q-value. Probabilistic quotient normalization (PQN) was used for sample normalization. Local polynomial regression fitting signal correction (QC-RLSC) was used as an effective method for data correction in metabolomics area data analysis.

LC-MS/MS based untargeted lipidomics

The nontargeted LC-MS/MS lipidomics analysis was performed using high resolution mass spectrometer Q Exactive (Thermo Fisher Scientific, USA) for data acquisition in both positive-ion and negative-ion mode. SPLASH Internal standards: (330707, SPLASHTM Lipidomix Mass Spec Standard, Avanti Polar Lipids) was used. To each sample, isopropanol and internal standard were added and subjected to centrifugation. Equal volume of each sample was mixed into a QC sample for the evaluation of the repeatability and stability of the LC-MS analysis. CSH C18 column (1.7 μm 2.1x100 mm, Waters) was used. The mobile phase consisted of solvent A (60% acetonitrile aqueous solution, 0.1% formic acid, 10 mM ammonium formate) and solvent B (10% acetonitrile aqueous solution, 90% Isopropanol, 0.1%

formic acid, 10 mM ammonium formate) under positive ion mode, and solvent A (60% acetonitrile aqueous solution, 10 mM ammonium formate) and solvent B (10% acetonitrile aqueous solution, 90% Isopropanol, 10 mM ammonium formate) under negative ion mode. Q Exactive mass spectrometer (Thermo Fisher Scientific, USA) was used to obtain MS1 and MS2 data. The MS scan method was in the range of m/z 200–2000. The parameters of ESI were, sheath gas of 40 L/min, aux gas of 10 L/min, spray voltage 3.80 in positive ion mode and 3.20 in negative ion mode, capillary temperature of 320℃ and aux gas heater temperature of 350℃. Lipid identification was performed by Software Thermo Scientific LipidSearch v4.1, and data were transferred to metaX for data preprocessing and subsequent analysis.

PCA (Principal Component Analysis), PLS-DA (Partial Least Squares Method-Discriminant Analysis), and VIP (Variable Importance in Projection) values were employed in the data analysis. For the univariate analysis, fold change analysis, T test and false discovery rate (FDR) correction were performed to obtain the fold change, p-value and q-value, respectively. The results were screened for differential lipid molecules with criteria set at VIP of the first two principal components of the PLS-DA model equaled or above 1, fold change equaled or above 1.2 or less than 0.83 and the p-value less than 0.05.

Joint-pathway analysis for proteomics and metabolic data

To examine the correlation between the differential expressed protein (DEPs) and metabolites, we performed joint pathway analysis using MetaboAnalyst 3.0, which enabled the visualization of significant genes and metabolites that were enriched in a particular pathway. Functional annotation databases were utilized based on the gene ontology (GO) networks.

Establish constitutive Rab27a knockout mice (B6/J-Rab27a-Cas9-KO)

Constitutive Rab27a knockout mice (B6/J-Rab27a-Cas9-KO) were obtained by CRISPR/Cas9 technology (GemPharmatech Co., Ltd.). CRISPR-Cas9 system was used to perform the genome editing in the mice by delivering guide RNA to the designated genomic site and knockout Rab27a expression. Knockout of Rab27a in the mouse was confirmed by genotyping. The primers sequences for genotyping PCR study were JS05042-Rab27a-5wt-t, forward (F1) 5’- AGGCTACACGTACTGTTTCAAGGG-3’ and reverse (R1) 5’- AAACCAACAGTGTCAGCCATGTGTC-3’, and JS15042-Rab27a-wt-t, forward (F2) 5’- AGCTTTGTGGATGCTAAGCAAGAC-3’ and reverse (R2) 5’- TCATCTTACCAGGTGCAGATGAG-3’. Western blot analysis was also used to validate the knockout of Rab27a protein in various adipose tissues and organs.

Injection of exosomes to B6/J-Rab27a-Cas9-KO mice

Eighty micrograms of VAT-Exos, SAT-Exos or EAT-Exos isolated from the respective adipose depots dissected from the DIO mice was injected into the B6/J-Rab27a-Cas9-KO mice *via* tail vein twice a week for 2 weeks. The mice were fed with control diet during the experiment. Equal volume of PBS served as control.

Results

Obesity has differential impacts on the protein profiles of the EAT-Exos, VAT-Exos and SAT-Exos

We used C57BL/6J mice to set up HFD-induced obesity (DIO) mouse model (Fig. 1a), control diet (CD) served as control. Exosomes derived from epididymal adipose tissue (EAT-Exos), visceral adipose tissue (VAT-Exos) and subcutaneous adipose tissue (SAT-Exos) were purified. Transmission electron microscopy (TEM) indicated the circulating exosomes were intact (Fig. 1b). TEM (Fig. 1b) and dynamic light scattering (DLS) (Fig. 1c) showed that the diameters of the purified exosomes were consistent with the proposed sizes of exosomes (30-150nm) [1]. Authenticity of the purified exosomes was also examined by the expressions of exosomal markers CD63 and CD81 (Fig. 1d).

iTRAQ-based quantitative proteomic was used to examine the protein profiles of the EAT-Exos, VAT-Exos and SAT-Exos under obesity conditions. Data showed that a total of 304 proteins were upregulated and 186 were downregulated in EAT-Exos (Fig. 1e); while 306 exosomal proteins were upregulated, and 273 were downregulated in VAT-Exos (Fig. 1f). Interestingly, HFD feeding had a great impact on the protein profiles in the SAT-Exos as 578 proteins were upregulated, and 310 proteins were downregulated (Fig. 1g). Besides, we also compared the exosomal protein profiles in SAT-Exos, VAT-Exos and EAT-Exos under CD and HFD conditions as shown in the supplementary Fig. 1a to 1f. With eukaryotic orthologous groups (KOG) annotation, we found that the detected proteins in these exosomes were mainly involved in cellular process and participate in binding activity (supplementary Fig. 1g). Among different cellular processes, 13.46% of the exosomal proteins was involved in metabolic process (Table 1) including carbohydrate metabolism, amino acid metabolism and lipid metabolism (Fig. 1h).

Obesity affects the metabolic associated proteins in SAT-Exos and VAT-Exos

We next compared the impacts of obesity on the protein profiles of EAT-Exos, VAT-Exos and SAT-Exos. Proteins with 1.2-fold change and Q-value less than 0.05 were determined as differentially expressed proteins (DEPs). Most of the DEPs in the EAT-Exos, VAT-Exos and SAT-Exos were cytosolic proteins (Supplementary Fig. 2a-c). Although pathway enrichment analysis showed that DEPs in EAT-Exos, VAT-Exos and SAT-Exos were mainly involved in metabolism (Fig. 2a to 2c), only 239 and 375 metabolic-associated DEPs were identified in EAT-Exos (Supplementary Fig. 2d) and VAT-Exos (Supplementary Fig. 2e), respectively, while 544 metabolic-associated DEPs were identified in SAT-Exos (Supplementary Fig. 2f). Scatter plot of the top 20 of KEGG enrichment RichFactor also revealed that DEPs in EAT-Exos were not only associated to metabolism but other biological processes (Fig. 2d). As shown in Fig. 2e, DEPs in EAT-Exos also involved in calcium metabolism, endocytosis, bacterial invasion and cortisol synthesis and secretion, endocrine and other factor-regulated calcium reabsorption, peroxisome and fatty acid metabolism. DEPs in VAT-Exos were mainly involved in complement and coagulation cascades, pathogenic bacterial infection and metabolism (Fig. 2f and 2g). Interestingly, DEPs in SAT-Exos were mostly involved in metabolism (Fig. 2h) with a few DEPS involved in proteasome (Fig. 2i).

Furthermore, we performed STRING to predict the protein-protein interaction (PPI) of the DEPs, which include both physical and functional associations. Interestingly, PPI of the DEPs in SAT-Exos predicted

that the upregulated DEPs mainly interacted with other DEPs that were upregulated, and downregulated DEPS with other DEPs that were downregulated, which was different from those in EAT-Exos and VAT-Exos (Supplementary Fig. 2g to 2i) We postulated that such DEPs interactions in SAT-Exos would exacerbate the pathological effects of the DEPs under obesity conditions. Supplementary Table 1a to 1c separately highlighted the DEPs in EAT-Exos, VAT-Exos and SAT-Exos that were increased by at least 2-fold or reduced by at least 0.3-fold. The results clearly showed that obesity had differential effects on the exosomal proteins in these exosomes.

Our proteomic data strongly suggest that obesity has a more prominent effect on the proteins in the SAT-Exos than those in EAT-Exos and VAT-Exos. The DEPs in the EAT-Exos are involved in different biological functions, while those in SAT-Exos and VAT-Exos are mainly involved in metabolism.

Untargeted metabolomics analysis reveals a significant impact of SAT-Exos on the serum metabolite profile in constitutive Rab27a knockout mouse model

Since the DEPs in SAT-Exos and VAT-Exos under obesity conditions are mainly related to metabolism, we next examined whether these exosomes would affect the metabolic profiles in the mice. To eliminate the effects of endogenous exosomes on the mouse metabolism, we used constitutive Rab27a knockout mouse (B6/J-Rab27a-Cas9-KO) as model. Rab27a is critical for exosome secretion [22]. More importantly, Rab27a-KO mice are shown to have reduced exosome secretion [23]. We first preformed genotyping to validate the knockout of Rab27a in the B6/J-Rab27a-Cas9-KO mice. As shown in Fig. 3a, only homozygous knockout mice were selected for the study. Knockout of Rab27a protein in adipose tissues, heart, liver, spleen, lung, kidney and brain was confirmed by Western blot analysis (Fig. 3b). These data clearly demonstrated that Rab27a, the critical protein for exosome secretion, was successfully knockout in the B6/J-Rab27a-Cas9-KO mice.

Then, we separately injected equal amount of EAT-Exos, VAT-Exos and SAT-Exos that were purified from DIO mice into the B6/J-Rab27a-Cas9-KO mouse models. The injections were done twice a week for 2 weeks. Then, we employed untargeted metabolomics analysis to examine the changes of the metabolite profiles in these mice. The quality of the samples was tested by chromatogram overlapping (Supplementary Fig. 3a and 3b) and the coefficient of variation (CV) of the relative peak area in the samples (Supplementary Fig. 3c). In the metabolomic study, a total of 1858 compounds were detected in the positive mode, and 739 of them with known identification. In the negative mode, only 561 compounds were detected and 315 of them with known identification. Most of the metabolites detected in the positive mode are amino acids and organic acids in the negative mode. KEGG database was used to annotate the identified metabolites to understand their biological functions. As shown in supplementary Fig. 3d and 3e, most of the metabolites were involved in amino acid metabolism, followed by lipid metabolism, carbohydrate metabolism and metabolism of cofactors and vitamins.

To examine the differential effects of the EAT-Exos, VAT-Exos and SAT-Exos on metabolism, we employed PLS-DA to examine the distribution and separation trend of the metabolite samples. PLS-DA provides high rates of sensitivity and specificity as it can substantially reduce the number of discriminatory

variables by creating significant VIP (variable importance in projection) scores. As revealed by the models, injections of SAT-Exos, EAT-Exos or VAT-Exos that were purified from DIO mice had significant impacts on the plasma metabolites in the B6/J-Rab27a-Cas9-KO mice as illustrated by the sample clustering in the PLS-DA (Supplementary Fig. 3f to 3h).

We next screened for the differential metabolites in different grouping pairs of the mice. In the screening process, VIP of the first two PCs of the PLS-DA model above 1 was set as one of the criteria; and only metabolites with fold changes ≥ 1.2 or ≤ 0.83 that reached statistical significance (p-value < 0.05) were shortlisted. As shown in Supplementary Table 2, EAT-Exos injection significantly affected a total of 47 metabolites, VAT-Exos injection affected a total of 62 metabolites, and SAT-Exos injection affected a total of 153 metabolites in both positive and negative modes. The metabolites detected in these mice were listed in Supplementary Table 3a to 3f. The visual displays of the differential metabolites were shown in the respective volcano plots (Fig. 3c to 3e) and heat maps (Supplementary Fig. 3i to 3k).

In the pathway enrichment analysis, only the metabolites that showed statistically significant differences between groups were shortlisted for the analysis. The number of affected pathways after EAT-Exos injection was less than those after VAT-Exos and SAT-Exos injections (Table 2a). Interestingly, injection of SAT-Exos affected many metabolic pathways in the mice with a total of 1706 differential metabolites involved (Table 2a).

We next correlated these differential metabolites after SAT-Exos injection with the DEPs in the SAT-Exos that were increased by at least 2-fold or reduced by 0.3-fold as listed in supplementary Table 1c. We found that these DEPs were correlated to 14 different metabolisms including amino acid metabolisms and lipid metabolisms such as fatty acid degradation and steroid hormone biosynthesis (Fig. 3f).

Taken together, the metabolomic data suggest that the effects of EAT-Exos, VAT-Exos and SAT-Exos on the mouse metabolism are different. Injection of SAT-Exos has more prominent effects on the metabolite profiles and metabolic pathways in the B6/J-Rab27a-Cas9-KO mice when compared to EAT-Exos and VAT-Exos injections. Correlation analysis suggest that DEPs in the SAT-Exos contribute to the metabolic changes including amino acid metabolism and fatty acid metabolism under obesity conditions.

Untargeted lipidomics analysis reveals the impacts of SAT-Exos on the plasma lipid profile in B6/J-Rab27a-Cas9-KO mouse model, which mimic the plasma lipid profile in DIO mice

Since our data suggest that SAT-Exos that are derived from DIO mice have significant effects on fatty acid metabolism, we next performed global lipidomics to compare the plasma lipid profiles between the DIO mice and the B6/J-Rab27a-Cas9-KO mice after SAT-Exos injection.

After injecting SAT-Exos purified from DIO mice into the B6/J-Rab27a-Cas9-KO mice twice a week for two weeks, we performed untargeted lipidomics with the plasma lipid samples. The base peak chromatograms (BPC) of the lipid samples in positive and negative modes were shown in supplementary Fig. 4a and 4b. The CV distribution of lipid molecules was shown in supplementary Fig. 4c. Multivariate

statistical analysis and univariate analysis were used to screen different lipids between groups. PLS-DA models showed the separation trends of the different plasma lipid samples, suggesting that SAT-Exos affects the plasma lipid profiles (supplementary Fig. 4d). Interestingly, SAT-Exos injection reduced the triglyceride (TG) levels, it also changed the levels of glycerophospholipids in the plasma in these mice (supplementary Table 4). Subsequent pathway enrichment analysis also suggests that SAT-Exos affects metabolism such as arachidonic acid metabolism, linoleic acid metabolism, biosynthesis of unsaturated fatty acid, regulation of lipolysis in adipocytes and glycerophospholipid metabolism in the mice (Table 2b).

Next, we examined the lipid profiles in the DIO mice, with CD mice served as control. The BPC of the lipid samples in the DIO and CD mice were shown in Supplementary Fig. 5a to 5d. In the lipidomic study, a total of 667 lipid molecules were detected. The lipid profiles for HFD and CD mice were different as indicated by the lipid sample clustering in the PCA (Supplementary Fig. 5e). The differences in the lipid molecules between these mice were visualized in volcano plots (Fig. 4a) and the heat maps (supplementary Fig. 5f), respectively.

Interestingly, our previous data showed that injection of SAT-Exos purified from DIO mice into the B6/J-Rab27a-Cas9-KO mice reduced TG levels and changed glycerophospholipid levels. DIO mice also exhibited similar changes when compared to CD mice. As shown in Fig. 4b, in the DIO mice, the levels of fatty acid (FA), diglyceride (DG), monoglyceride and diglyceride (MGDG) were increased, while TG level was reduced (Fig. 4b), which suggest a change in the lipolytic activity. Besides, SAT-Exos also changed the plasma levels of glycerophospholipids including dimethylphosphatidylethanolamine (dMePH), phosphatidylserine (PS), lyso-phosphatidylglycerol (LPG), phosphatidylglycerol (PG), lyso-phosphatidylcholine (LPC), phosphatidylethanolamine (PE), lyso-phosphatidylethanolamine (LPE), phosphatidylglycerol (PI), lysodimethylphosphatidylethanolamine (LdMePE) and phosphatidylcholine (PC).

Discussion

This is the first few reports comparing the protein profiles in EAT-Exos, VAT-Exos and SAT-Exos under obesity conditions. Our data show that obesity has a more prominent effect on the protein profiles in SAT-Exos than those in EAT-Exos and VAT-Exos. Interestingly, DEPs in SAT-Exos and VAT-Exos are mainly involved in metabolism. Subsequent metabolomics and lipidomics suggest that SAT-Exos contribute to the changes in the lipid metabolism such as the fatty acid and glycerophospholipid metabolism under obesity conditions.

Dysregulation of fatty acid disposition and ectopic lipid accumulation in organs and tissues is a major contributing factor to metabolic syndrome under obesity conditions [24]. Clinical and epidemiological findings show that obese patients more likely to develop metabolic complications [25], which is in part, due to the abnormalities in lipid metabolism [26]. The elevated circulating fatty acid level is a key pathophysiological feature in the obese patients [27]. These elevated fatty acids affect the secretion of

adipokines and inflammatory cytokines [26]. In obese patients, the circulating palmitic acid has a positive correlation with the levels of C-reactive protein ($r = 0.2965$; $p = 0.035$) [26] that is an acute marker of inflammation [29]. Many studies have explored the mechanism underlying the elevated circulating fatty acid levels in the obese patients. It has been suggested that under obesity conditions, adipocytes are having hypertrophic and hyperplastic growth. The hypertrophic adipocytes develop insulin resistance, hence increases lipolysis and fatty acid flux from the adipose tissues to the circulation [28]. Besides, pro-inflammatory signal such as tumor necrosis factor-alpha or some adipokines [25] will also induce insulin resistance and enhance lipolysis in the adipocytes.

Our data have identified the DEPs in the SAT-Exos under obesity conditions; among these, 16 DEPs are upregulated by more than 2 folds, and 19 DEPs are reduced by more than 0.3 folds under obesity conditions. By correlating these DEPs and the metabolic profiles of B6/J-Rab27a-Cas9-KO mice after injecting the SAT-Exos, we suggest that the DEPs in SAT-Exos may contribute to the metabolic changes under obesity. Some of these metabolic changes are amino acid metabolism while others are lipid metabolism including fatty acid degradation and steroid hormone biosynthesis. With focus on the lipid metabolism, we then performed lipidomics with DIO mice, and we indeed observe the changes in the plasma levels of fatty acids and glycerophospholipids in the mice.

Among the DEPs in the SAT-Exos, ADP-ribosylation factor (Arf) is elevated by 2.1 folds in the SAT-Exos under obesity conditions. Other study has shown that Arf protein levels are markedly increased in the white adipose tissues in ob/ob mice, whereas they are decreased in obesity-resistant mice [30]. More importantly depletion of Arf inhibits isoproterenol-stimulated lipolysis in adipocytes, which is independent of insulin signaling [30]. Besides, Arf also mediates the endothelin-1 induced lipolysis in the adipocytes [31]. A study shows that endothelin-1 induces lipolysis by activating Arf and extracellular signal-regulated kinases (ERK) in adipocytes, which can be inhibited by the inhibitors of Arf and ERK [31]. Given the lipolytic role of Arf, the elevated level of Arf in the SAT-Exos may underly the enhanced lipolysis in the adipocytes under obesity conditions.

Besides, mitogen-activated protein kinase kinase kinase 3 (MAP3K) is upregulated by 4.49 folds in the SAT-Exos under obesity conditions. MAP3K is a serine/threonine specific protein kinase, it activates MAP2K that in turns activates MAPK. Other protein kinases involved in the MAPK signaling cascade are ERK1/2, the c-JUN N-terminal kinase 1, 2 and 3 (JNK1/2/3), and the p38 MAPK. Study shows that MAP3K mix-lineage kinase 3 (MLK3) knockout mice are resistant to high fat diet-induced obesity, which is due to the inhibition of obesity-induced JNK activation, reduction in macrophage infiltration into adipose tissue and proinflammatory cytokine expressions [32]. Therefore, MAP3K activity contributes to the obesity pathophysiology. However, whether the elevation of MAP3K in the SAT-Exos under obesity conditions contributes to the changes in the plasma levels of fatty acids and glycerophospholipids is yet unknown. Other studies also show that MAPK signaling pathways are associated with the development of liver steatosis [33–34] and hepatocellular carcinoma [35], further studies can be done to investigate the involvement of the elevated level of MAP3K in SAT-Exos in the disease development.

Our data also show that, unlike the DEPs in EAT-Exos, those in the SAT-Exos and VAT-Exos are mainly involved in metabolism under obesity conditions. In general, it is believed that excessive VAT is a risk factor for metabolic diseases [36]. VAT is directly associated with systemic inflammation by secreting various cytokines [37–38], which leads type 2 diabetes, atherosclerosis, cardiovascular disease, and some cancers [39–41]. However, study also suggests that the altered fatty acid metabolism under obesity conditions is not a direct consequence of VAT activity, but a dysfunction of SAT in which the abdominal SAT fails to adapt and expand through hyperplasia to store the excess circulating fatty acids [42]. Our study may reveal a novel role of SAT and SAT-Exos in changing the fatty acid metabolism under obesity conditions, which may suggest therapeutic targets for the treatment of obesity and its associated comorbidities.

Besides, based on our data, the role of EAT-Exos in contributing to the metabolic changes under obesity conditions is less prominent. DEPs in EAT-Exos under obesity conditions are involved in various signaling pathways including melanogenesis, Fc gamma R-mediated phagocytosis, calcium signaling pathway, regulation of actin cytoskeleton, gastric acid secretion. Although some of the DEPs in EAT-Exos are involved in metabolism such as carbon metabolism and fatty acid metabolism, injection of EAT-Exos into the B6/J-Rab27a-Cas9-KO mice does not profoundly affect the mouse metabolism. Indeed, the association of EAT and obesity or its comorbid conditions is less reported.

In conclusion, our data strongly suggest that obesity has more prominent effects on the protein profile of the SAT-Exos. DEPs in SAT-Exos may contribute to the altered fatty acid metabolism under obesity conditions. Our study has paved the way for the future development of novel exosome-based therapeutics for the treatment of obesity.

Declarations

Author Contributions

M.C., F. Z. and B.C. carried out the experiments and preformed the data analysis in this study. C.H. performed the TEM and DLS in this study. C.L., Q.H., T.S. and H.Y. Kwan designed the experiments and study. T.S. and H.Y. Kwan wrote the manuscript.

Funding

This work was partially supported by Shenzhen Virtual University Park (SZVUP) Special Fund Project #2021Szvup131, FNRA-IG (RC-FNRA-IG/20-21/SCM/01), ITC (PRP/015/19FX), GDNSF (2021A1515010655) and HMRF (08193596) to HYK; and Characteristic Innovation Projects of Universities in Guangdong Province (2020KTSCX030), Administration of Traditional Chinese Medicine of Guangdong Province (20222042) to ST.

Ethics approval

The animal studies were approved by the Research Ethics Committee at Hong Kong Baptist University and the Department of Health in the Hong Kong Special Administration Region.

Consent for publication

Have informed consent for publication

Availability of data and material

Online version contains supplementary materials. All the data are available from the corresponding authors upon reasonable request.

Acknowledgements

We thank the Centralized Research Facilities, The Science and Engineering Core Service at Hong Kong University for providing the TEM facilities. We thank the BGI Genomics for providing the facilities and service for the omics studies.

Conflict of interest

The authors declare no competing interests.

References

1. Pegtel DM, Gould SJ (2019) Exosomes. Annu Rev Biochem 88:487–514
2. Kalluri R, LeBleu VS (2020) The biology, function, and biomedical applications of exosomes. Science 367:eaau6977
3. Connolly KD et al (2015) Characterisation of adipocyte-derived extracellular vesicles released pre- and post-adipogenesis. J Extracell Vesicles 4:29159
4. Wen Z et al (2020) Hypertrophic Adipocyte-Derived Exosomal miR-802-5p Contributes to Insulin Resistance in Cardiac Myocytes Through Targeting HSP60. Obesity 28:1932–1940
5. Sano S et al (2014) Lipid synthesis is promoted by hypoxic adipocyte-derived exosomes in 3T3-L1 cells. Biochem Biophys Res Commun 445:327–333
6. Deng ZB et al (2009) Adipose tissue exosome-like vesicles mediate activation of macrophage-induced insulin resistance. Diabetes 58:2498–2505
7. Kwan HY et al (2021) The impact of obesity on adipocyte-derived extracellular vesicles. Cell Mol Life Sci 78(23):7275–7288
8. Samuelson I, Vidal-Puig AJ (2018) Fed-EXosome: Extracellular vesicles and cell–cell communication in metabolic regulation. Essays Biochem 62:165–175
9. Gao X, Salomon C, Freeman DJ (2017) Extracellular Vesicles from Adipose Tissue-A Prominential Role in Obesity and Type 2 Diabetes? Front. Endocrinol 8:202

10. Akbar N, Azzimato V, Choudhury RP, Aouadi M (2019) Extracellular vesicles in metabolic disease. Diabetologia 62:2179–2187
11. Li CJ, Fang QH, Liu ML, Lin JN (2020) Current understanding of the role of Adipose-derived Extracellular Vesicles in Metabolic Homeostasis and Diseases: Communication from the distance between cells/tissues. Theranostics 10:7422–7435
12. Kita S, Maeda N, Shimomura I (2019) Interorgan communication by exosomes, adipose tissue, and adiponectin in metabolic syndrome. J Clin Invest 129:4041–4049
13. Deng Z et al (2009) Adipose tissue exosome-like vesicles mediate activation of macrophage-induced insulin resistance. Diabetes 58:2498–2505
14. Müller G et al (2011) Microvesicles released from rat adipocytes and harboring glycosylphosphatidylinositolanchored proteins transfer RNA stimulating lipid synthesis. Cell Signal 23(7):1207–122322
15. Kwok KHM, Lam KSL, Xu A (2016) Heterogeneity of white adipose tissue: molecular basis and clinical implications. Exp Mol Med 48:e215
16. Gerhard GS et al (2014) Gene expression profiling in subcutaneous, visceral and epigastric adipose tissues of patients with extreme obesity. Int J Obesity 38:371
17. Schleinitz D, Bottcher Y, Bluher M, Dovacs P (2014) The genetics of fat distribution. Diabetologia 57:1276
18. Hartwig S et al (2019) Exosomal proteins constitute an essential part of the human adipose tissue secretome. Biochim Biophys Acta Proteins Proteom 1867(12):140172
19. Lazar I et al (2016) Adipocyte Exosomes Promote Melanoma Aggressiveness through Fatty Acid Oxidation: A Novel Mechanism Linking Obesity and Cancer. Cancer Res 76(14):4051
20. Purushothaman A (2019) Exosomes from Cell Culture-Conditioned Medium: Isolation by Ultracentrifugation and Characterization. Methods Mol. Biol. 1952: 233–244
21. Jung MK, Mun JY (2018) Sample Preparation and Imaging of Exosomes by Transmission Electron Microscopy. J Vis Exp 131:67482
22. Ostrowski M et al (2010) Rab27a and Rab27b control different steps of the exosome secretion pathway. Nat Cell Biol 12(1):19
23. Hu M et al (2018) The harsh microenvironment in infarcted heart accelerates transplanted bone marrow mesenchymal stem cells injury: the role of injured cardiomyocytes-derived exosomes. Cell Death Dis 9:357
24. Verna EC, Berk PD (2008) Role of fatty acids in the pathogenesis of obesity and fatty liver: impact of bariatric surgery. Semin Liver Dis 28(4):407–426
25. Roche HM (2005) Fatty acids and the metabolic syndrome. Proc Nutr Soc 64(1):23–29
26. Lottenberg AM et al (2012) The role of dietary fatty acids in the pathology of metabolic syndrome. J Nutr Biochem 23:1027

27. Guerendiain M et al (2018) Changes in plasma fatty acid composition are associated with improvements in obesity and related metabolic disorders: A therapeutic approach to overweight adolescents. Clin Nutr 37(1):149–156
28. Wrzosek M et al (2022) Impact of Fatty Acids on Obesity-Associated Diseases and Radical Weight Reduction. Obes Surg 32:428–440
29. Clos TW, Du (2000) Function of C-reactive protein. Ann Med 32(4):274–248
30. Liu Y et al (2010) ADP-ribosylation factor 6 modulates adrenergic stimulated lipolysis in adipocytes. Am J Physiol Cell Physiol 298(4):C921
31. Davies JCB et al (2014) ADP-ribosylation factor 6 regulates endothelin-1-induced lipolysis in adipocytes. Biochem Pharmacol 90(4):406–413
32. Gadang V et al (2013) MLK3 promotes metabolic dysfunction induced by saturated fatty acid-enriched diet. Am J Physiol Endocrinol Metab 305(4):E549–556
33. Cicuendez B et al (2021) Stress kinases in the development of liver steatosis and hepatocellular carcinoma. Mol Metab 50:101190
34. Donohoe F et al (2020) Mitogen-Activated Protein Kinase (MAPK) and Obesity-Related Cancer. Int J Mol Sci 21(4):1241
35. Wang L et al (2016) Mitogen-activated protein kinase kinase 3 induces cell cycle arrest via p38 activation mediated Bmi-1 downregulation in hepatocellular carcinoma. Mol Med Rep 13:243–248
36. Fox CS et al (2007) Abdominal visceral and subcutaneous adipose tissue compartments: association with metabolic risk factors in the framingham heart study. Circulation 116:39–48
37. Fontana L et al (2007) Visceral fat adipokine secretion is associated with systemic inflammation in obese humans. Diabetes 56:1010–1013
38. Choi CHJ, Cohen P (2017) Adipose crosstalk with other cell types in health and disease. Exp Cell Res 360:6–11
39. de Jong PE et al (2002) Obesity and target organ damage: the kidney. Int J Obes Relat Metab Disord 26(Suppl 4):S21–S24
40. Ji C, Guo X (2019) The clinical potential of circulating microRNAs in obesity. Nat Rev Endocrinol 15:731–743
41. Liu Y et al (2021) Multifaceted Roles of Adipose Tissue-Derived Exosomes in Physiological and Pathological Conditions. Front Physiol 12:669429
42. Marcadenti A et al (2015) Different adipose tissue depots: Metabolic implications and effects of surgical removal. Endocrinol Nutr 62(9):458

Tables

Tables 1 to 2 are available in the Supplementary Files section.

Figures

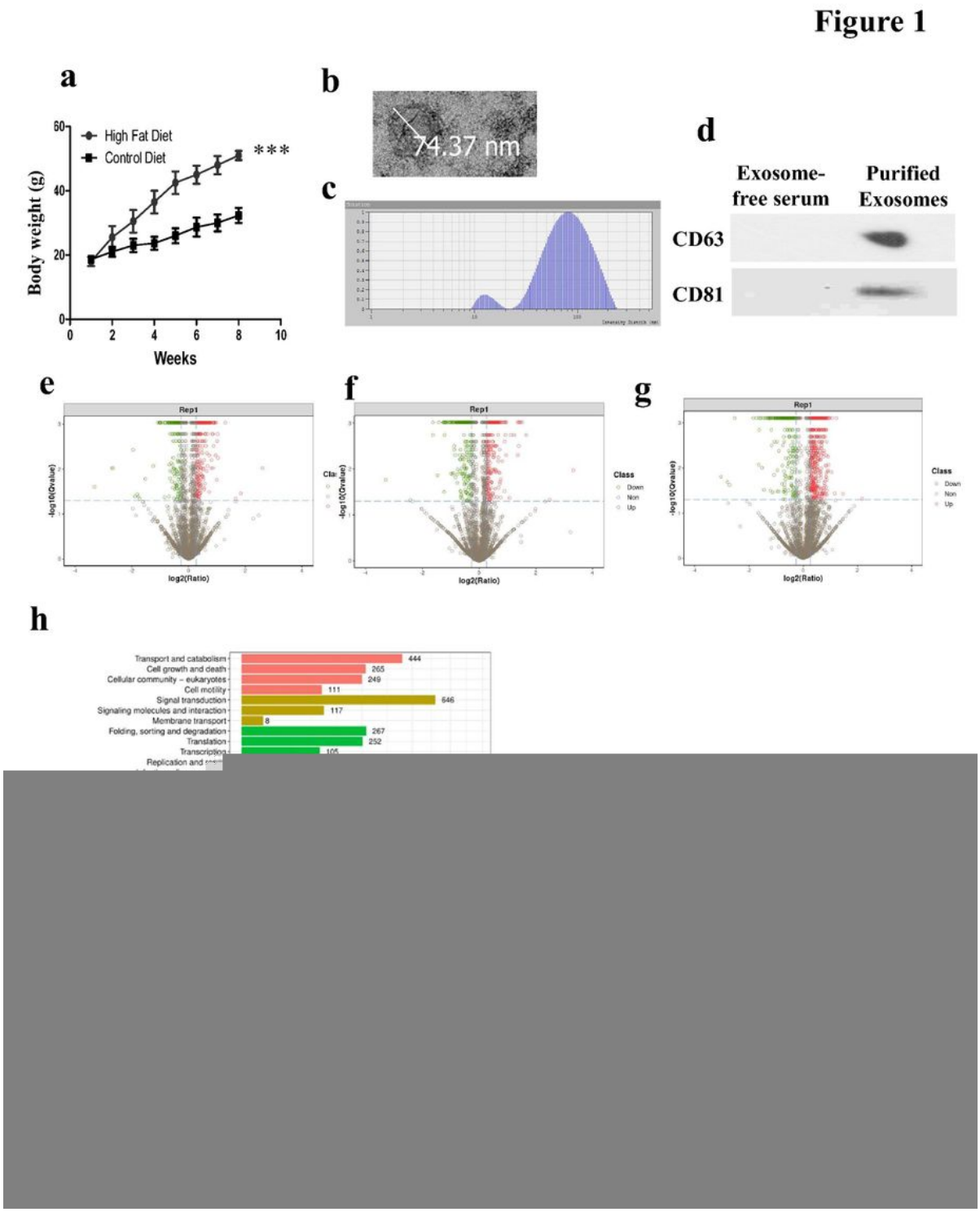

Figure 1

Obesity has differential impacts on the protein profiles of the EAT-Exos, VAT-Exos and SAT-Exos. (a) The body weight of high fat diet induced (DIO) obesity mice and control diet (CD) mice. (**b)** TEM and (**c)** DLS analysis of the purified exosomes. **(d)** Expressions of CD63 and CD81 proteins in the purified exosomes. Volcano plots showing the up-regulated and down-regulated proteins in the **(e)** EAT-Exos, **(f)** VAT-Exos and **(g)** SAT-Exos under obesity conditions; and the **(h)** pathway analysis of the detected exosomal proteins.

EAT-Exos, exosomes derived from epididymal adipose tissue; VAT-Exos, exosomes derived from visceral adipose tissue; SAT-Exos, exosomes derived from subcutaneous adipose tissue of the DIO mice. n = 3-4 mice in each group.

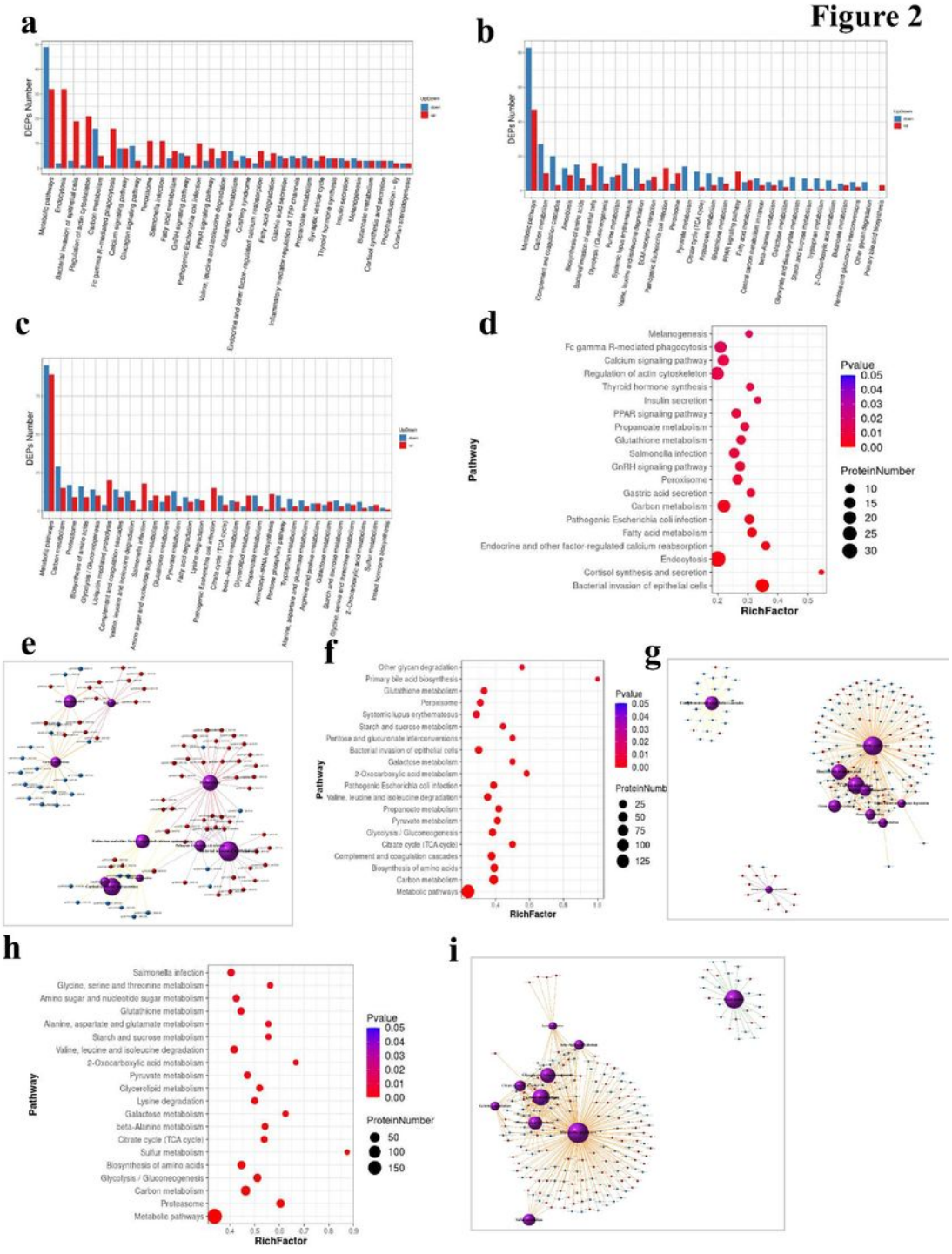

Figure 2

Obesity affects the metabolic associated proteins in SAT-Exos and VAT-Exos. Pathway enrichment analysis of the differentially expressed proteins (DEPs) in the **(a)** EAT-Exos, **(b)** VAT-Exos and **(c)** SAT-Exos under obesity conditions. Statistics of pathway enrichment of DEPs in **(d)** EAT-Exos, **(f)** VAT-Exos and **(h)** SAT-Exos under obesity conditions; and the network analysis of the pathway terms for the DEPs in the **(e)** EAT-Exos, **(g)** VAT-Exos and **(i)** SAT-Exos. EAT-Exos, exosomes derived from epididymal adipose tissue; VAT-Exos, exosomes derived from visceral adipose tissue; SAT-Exos, exosomes derived from subcutaneous adipose tissue of the DIO mice. n = 3-4 mice in each group.

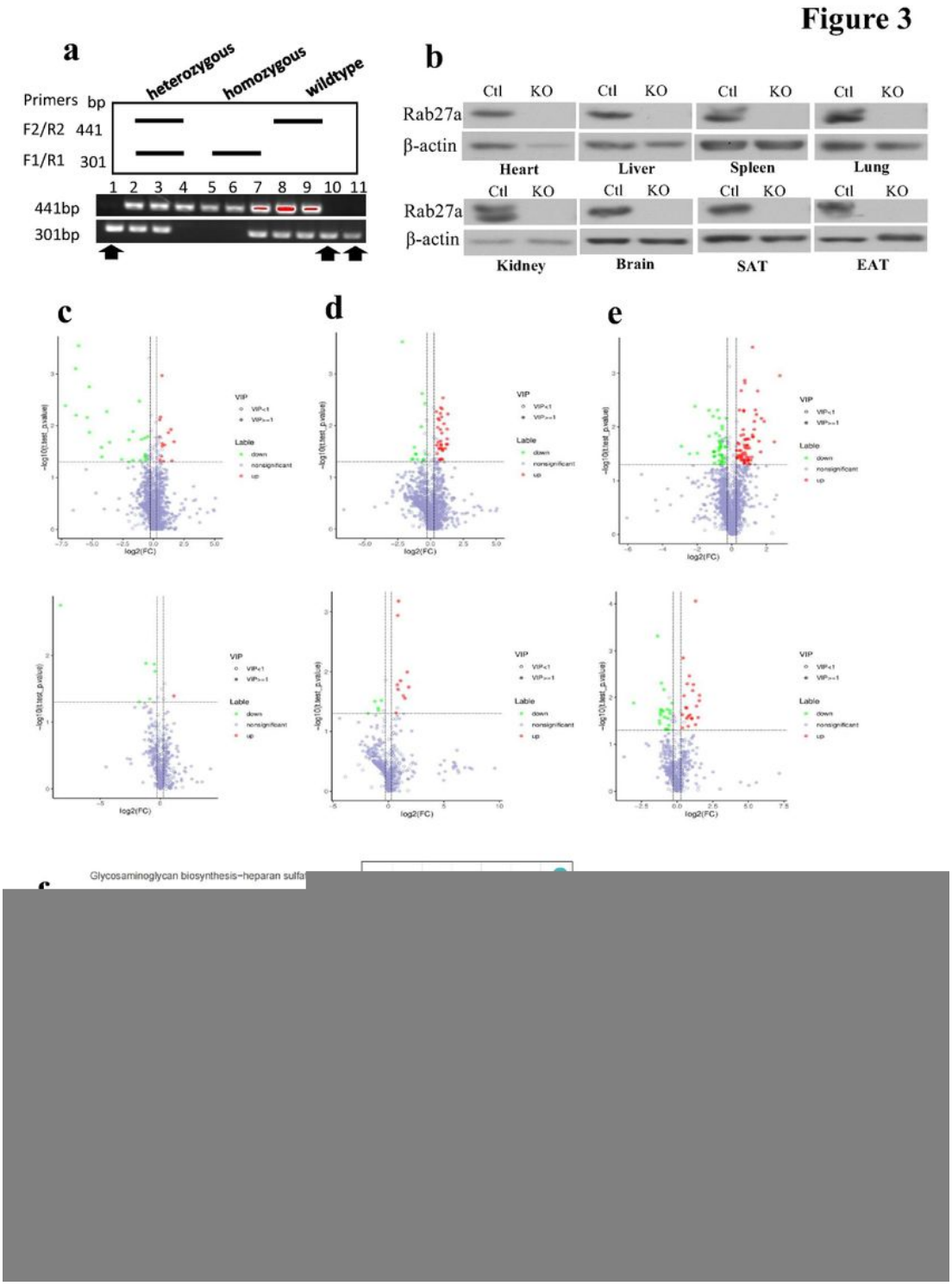

Figure 3

Untargeted metabolomics analysis reveals the impact of SAT-Exos on the serum metabolite profile in constitutive Rab27a knockout mouse model

(a) Genotyping of the male Rab27a knockout mice (B6/J-Rab27a-Cas9-KO) and **(b)** expressions of Rab27a protein in the heart, liver, spleen, lung, kidney, brain, subcutaneous adipose tissue (SAT) and epididymal adipose tissue (EAT) in the homozygous knockout mice. Volcano map of the differential metabolites in **(c)** EAT-Exos, **(d)** VAT-Exos and **(e)** SAT-Exos (upper panel, positive ion mode; lower panel, negative ion mode) under obesity conditions. **(f)** Correlation analysis of the differential metabolites in the B6/J-Rab27a-Cas9-KO mice after SAT-Exos injection and the differential expressed proteins in the SAT-Exos derived from high fat diet induced (DIO) mice. n = 3-4 mice in each group.

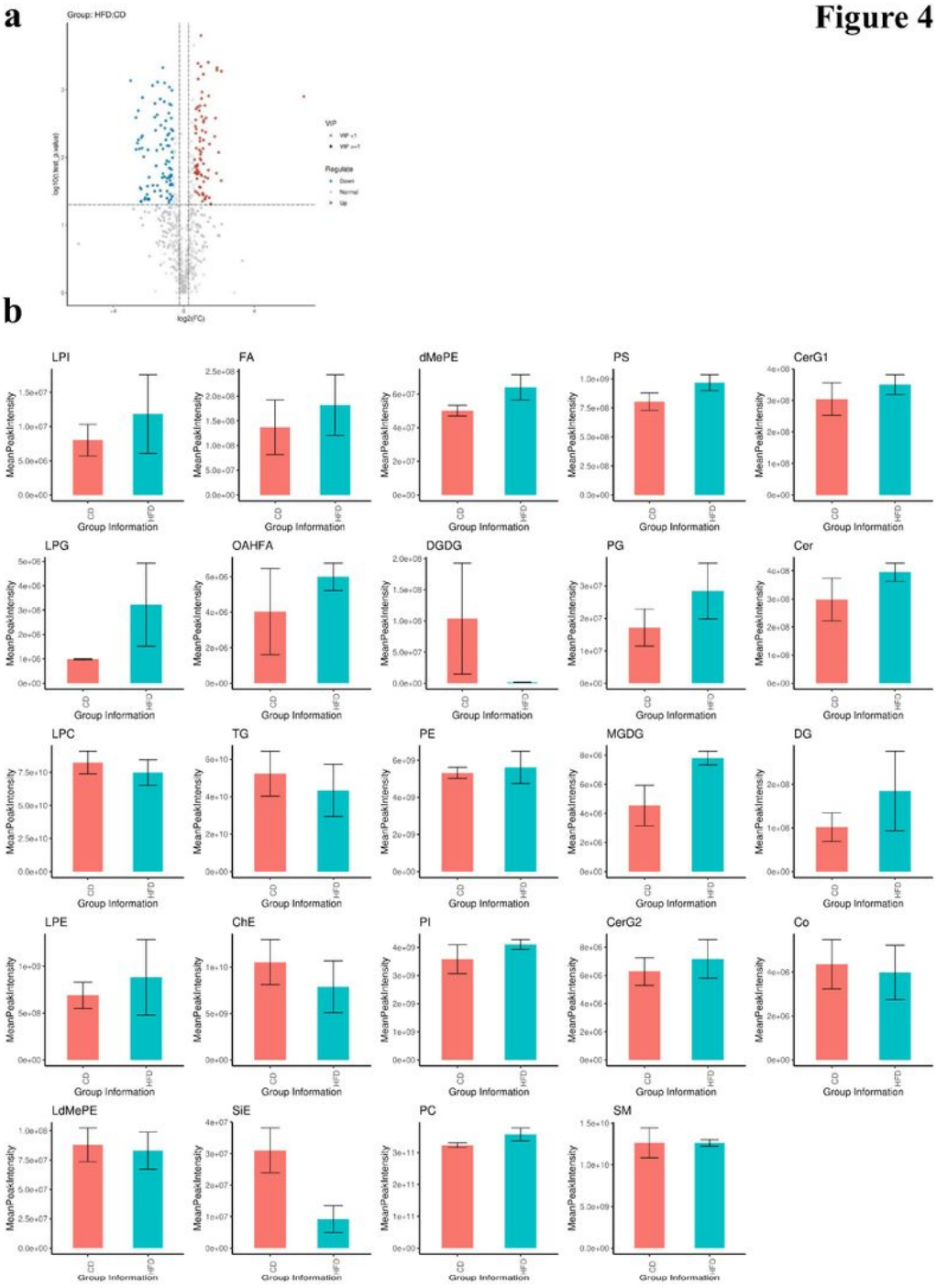

Figure 4

Untargeted lipidomics analysis of the plasma lipid profile in B6/J-Rab27a-Cas9-KO mice after SAT-Exos injection, and the plasma lipid profile in DIO mice

(a) The volcano map of differential metabolites and the **(b)** detected changes in lipid sub-classes in the B6/J-Rab27a-Cas9-KO mice after injecting SAT-Exos derived from high fat diet induced (DIO) mice. n = 3-

4 mice in each group.

Supplementary Files

This is a list of supplementary files associated with this preprint. Click to download.

- SupplementaryFigures15.pdf
- SupplementaryTable1a.xlsx
- SupplementaryTable1b.xlsx
- SupplementaryTable1c.xlsx
- SupplementaryTable2.xlsx
- SupplementaryTable3a.xlsx
- SupplementaryTable3b.xlsx
- SupplementaryTable3c.xlsx
- SupplementaryTable3d.xlsx
- SupplementaryTable3e.xlsx
- SupplementaryTable3f.xlsx
- SupplementaryTable4.xlsx
- Table1.xlsx
- Table2a.xlsx
- Table2b.xlsx